Environmental Microbiology (2005) **7**(8), 1085–1103 doi:10.1111/j.1462-2920.2005.00787.x

A framework for multidimensional modelling of activity and structure of multispecies biofilms

Joao B. Xavier,* Cristian Picioreanu and Mark C. M. van Loosdrecht
Department of Biotechnology, Delft University of Technology, Julianalaan 67, 2628 BC Delft, the Netherlands.

Summary

Concepts from previous biofilm models were integrated to create a framework for the implementation of multidimensional (2D and 3D) multispecies biofilm models. The framework is here described at three levels: (i) mathematical representation of the processes involved in biofilm formation, (ii) numerical implementation into a computer program (freely available from our website http://www.biofilms.bt.tudelft.nl/frameworkMaterial) and (iii) using the program for the creation of biofilm models with multiple bacterial and solute species. An improved version of the individual-based modelling (IbM) that allows structured biomass was used. In this approach biomass composition may be discriminated into any number of particulate species, including extracellular polymeric substances (EPS) for which specific functionality was included. Detachment is also included, described as occurring at the biofilm surface with variable local rates derived from functions of state variables. The application of this modelling framework to a multispecies system with structured biomass is illustrated in a case study where the competition between an organism capable of accumulating polyhydroxybutyrate (PHB, an internal storage compound) and an EPS-producing organism in a two-species biofilm is analysed. Results illustrate that biofilms enriched in PHB-producing organisms may be obtained by supplying substrate intermittently in feast/famine cycles.

Introduction

Biofilm research has been motivated by the goal of controlling biofilms, from the hindering of biofilm-related infections and harmful biofouling of industrial equipment to the tailoring of biofilms for specific applications, as in water and wastewater treatment and the fixed film fermenters in biotechnology industries. In order to fully understand biofilm dynamics, the basic processes involved in their formation and growth must be understood. Among other aspects, this implies understanding the characteristics of mass transfer processes in biofilms, notably different from those occurring for planktonic bacterial cells. In biofilms, fluid flow is greatly reduced and diffusional distances are frequently long enough to produce significant solute gradients. In these conditions, mass transport may become the rate limiting process of the various biotransformations occurring (Characklis and Marshall, 1990). Solute gradients account for the formation of microniches inside the biofilm matrix (Kuenen *et al*., 1986), requiring knowledge of the microenvironment in order to interpret biofilm behaviour from the extrapolation of the kinetics of individual cells.

The biofilm structure is here defined as the three-dimensional shape of the biofilm matrix and the spatial distribution of biotic and abiotic substances in this biofilm matrix. Biofilm structure is likely to play an important role in conditioning the activity of a biofilm. Experimental studies (Zhang *et al*., 1994; Wasche *et al*., 2002) as well as modelling studies (Rittmann *et al*., 1999; Picioreanu *et al*., 2000a; Klapper, 2004) indicate that the shape of the biofilm surface, i.e. the interface through which mass transfer between the biofilm and the environment takes place, influences biofilm activity significantly. The spatial distribution of substances in the biofilm matrix refers to the distribution of biomass components such as bacterial cells of different species (and at diverse phases of development), extracellular polymeric substances (EPS) and inorganic materials. The biomass distribution possibly influences the rates of solutes transport and bioconversions (i.e. biofilm activity).

Biofilm activity, in turn, is likely to influence biofilm structure. Factors such as the rate of biomass growth and EPS production rate determine the growth of the biofilm matrix (Zhang and Bishop, 2001). In addition to the biofilm activity, external factors causing biomass detachment such as shear forces and other mechanical stresses also play an important role in the development of the biofilm structure (Kwok *et al*., 1998). Understanding this intricate relationship between the structure and the activity of a biofilm is crucial for effective control of biofilms in both industrial and medical settings (Stoodley *et al*., 1999).

Received 6 July, 2004; revised 1 November, 2004; accepted 8 November, 2004. *For correspondence. E-mail J.Xavier@tnw.tudelft.nl; Tel. (+31) 0 15 2781551; Fax (+31) 0 15 2782355.

Biofilm modelling aims to describe the dynamics of biofilm behaviour from a formal description of the physical, chemical and biological processes involved. By using this approach, any resulting interdependence of these processes should be an emergent characteristic rather than imposed as a precondition. A model that describes the dynamics of biofilm activity and structure from environmental conditions is a valuable tool for testing hypotheses, as parameters for the operation of experimental biofilm systems tend to affect each other often in non-linear ways. Biofilm models provide a clean way to study '*in silico*' the effect of direct changes to particular operation parameters that could not be carried out through experimentation (Van Loosdrecht *et al*., 2002).

One-dimensional (1D) biofilm models, such as the stratified dynamic multispecies model introduced by Wanner and Gujer (Wanner and Gujer, 1986; Wanner and Reichert, 1996) and implemented in the AQUASIM software (Reichert, 1994), are widely used to describe macroscopic conversions in biofilm systems and to predict biofilm processes in a quantitative way. Modelling of biofilm structure is possible using these models, although restricted to 1D vertical gradients. The validity of 1D models is based on the rationale that gradients in biofilms are orders of magnitude higher in the direction perpendicular to the attachment surface than in directions parallel to it. However, a number of important characteristics that derive from the dynamics of biofilm structure must be assumed. External and internal mass transfer coefficients, changes in pore volume and mobility of bacterial species in the biofilm matrix are examples of properties that must be explicitly defined.

Multidimensional (2D or 3D) models offer the potential to derive such properties implicitly derived from basic principles. Several approaches to multidimensional modelling of biofilm structures can presently be found in the literature (see Picioreanu and Van Loosdrecht, 2003 and Picioreanu *et al*., 2004 for a review). The individual-based modelling (IbM) approach (Kreft *et al*., 1998, 2001) provides a representation of the biomass as being composed by multiple spherical agents that act independently, analogously to how bacterial biofilms are composed by multiple individual bacterial cells. In this bottom-up approach, the behaviour of the agents is defined explicitly with a set of rules that mimics the behaviour of individual bacterial cells, i.e. growth through the consumption of substrate, reproduction through cell division, production of metabolites, etc. Large-scale dynamics of the simulated biofilm is implicitly derived as an emergent property of the interactions between the agents (microorganisms) as they grow and reproduce. IbM has been applied previously to the modelling of bacterial colony growth (Kreft *et al*., 1998), multispecies biofilms (Kreft *et al*., 2001; Picioreanu *et al*., 2004), EPS formation by biofilms (Kreft and Wimpenny, 2001) and the development of altruistic behaviour by bacteria in biofilms (Kreft, 2004).

The approach proposed here extends on concepts integrated from previous modelling work (Picioreanu *et al*., 1998, 1999, 2001, 2004; Kreft and Wimpenny, 2001; Kreft *et al*., 2001) to provide a framework where any type of microbe/food kinetic interaction may be implemented, together with any number of solute and particulate species involved. A number of previous approaches to multidimensional modelling of biofilms have provided structured or multispecies descriptions of biomass (Noguera *et al*., 1999, 2000; Kreft and Wimpenny, 2001; Laspidou and Rittmann, 2004; Noguera and Picioreanu, 2004; Picioreanu *et al*., 2004), discriminating biomass constituents such as multiple bacterial species, inert biomass and EPS. The present framework accommodates the recognized necessity for modelling structured biomass with arbitrary numbers of components and extends the IbM to account for structured biomass. This allows any number of particulate species to be defined and the biomass composition in the models created using this framework may be as detailed as necessary. Specific methods for EPS production and excretion following a previously described approach (Kreft and Wimpenny, 2001) are also included.

The detachment of biomass from the biofilm is the main process balancing a positive biofilm growth (Stewart, 1993). Therefore, detachment is of chief importance in determining parameters that influence biofilm activity and composition such as steady-state biofilm accumulation (Van Loosdrecht *et al*., 1995) and average solids retention time of the biofilm (Morgenroth and Wilderer, 1999, 2000). Recognizing the importance of detachment in the development of biofilms, a biomass detachment description was here integrated with the IbM. The detachment model included is flexible to allow the application of a diversity of biomass detachment scenarios.

This integrated mathematical description of the processes involved in biofilm formation was used to produce a computer program for the creation of multidimensional biofilm models. The term multidimensional is used here in the sense that the framework allows time-dependent simulations to be carried out in either 2D or 3D spaces. All routines implemented in the program work in both 2D and 3D, and therefore the choice of the dimensionality of the simulations to be carried out is left to the user. The program is available in the form of a library of compiled Java classes from our website (Xavier *et al*., 2004a) at http://www.biofilms.bt.tudelft.nl/frameworkMaterial/ and may be readily used to create new multispecies biofilm models. The website also contains material to complement this article, including videos of the simulations presented in the case study section, as well as an interactive demonstration of the program.

Description of the biofilm modelling framework

Mathematical description of processes involved in biofilm formation

Reaction rates for involved species. A factor of chief importance in the present model is the classification of the involved species as either *particulate species* or *solute species*. In this classification, previously adopted by a well-established 1D biofilm model (Wanner and Gujer, 1986; Wanner and Reichert, 1996), particulate species include any substances composing the biofilm matrix, and solute species are the compounds dissolved in the liquid phase. Examples of particulates are active biomass of different bacterial species, inert biomass, internal storage products such as glycogen or lipids, and EPS. The dynamics for particulates include production or consumption resulting from bioconversions and advective transport caused by the spreading of the biofilm. Solutes are any dissolved substrate or microbial product relevant to the system. Examples include dissolved oxygen, carbon sources (e.g. glucose, acetate, etc.), nitrogen sources or substances involved in intercellular signalling. The solute species are also consumed or produced in bioreactions. Transport of solutes, however, occurs by diffusion, either through the biofilm or in the surrounding liquid medium.

A bioconversion process such as the growth of a bacterial species, endogenous respiration processes or the production of internal storage compounds, EPS or other, is here defined as a reaction involving any number of substrates and metabolic products. The substrates (consumed in the reaction) and metabolic products (produced in the reaction) of a reaction can be any species, solute or particulate, in the system. Reactions defined in this framework have reaction rates of first order to the concentration of the particulate species that mediates the reaction. As an example, growth rate of biomass is usually represented as first order to the concentration of the biomass species. The rates are defined in terms of the mass of a reference species, either solute or particulate, which is typically a species involved in the process as a substrate or a product. The following expression is the rate of a reaction $i(r_i)$ mediated by particulate species p:

$$r_i = q_i C_p \quad [M_m L^{-3} T^{-1}] \tag{1}$$

The rate is defined in concentration of the reference species m. The reference species m and the particulate species that mediates the reaction, p, may or may not be the same species. The coefficient q_i is the specific rate of the reaction i, defined in units of mass of the reference species m per mass of particulate species p per unit time, $M_m M_p^{-1} T^{-1}$, always having positive values. C_p is the concentration of particulate species p.

The specific reaction rate q_i is, in turn, defined as the product of a maximum specific rate, $q_i^{\max}$, and a series of factors, here represented generically by ϕ_j. These factors are typically saturation factors involving a function of the concentration C_j of a solute j having the form

$$\varphi_{M,j} = \frac{C_j}{C_j + K_j} \quad \text{[dimensionless]} \tag{2}$$

where K_j is called the half saturation constant (Monod limitation factor), or inhibition factors, which have the form

$$\varphi_{I,j} = \frac{K_j}{C_j + K_j} \quad \text{[dimensionless]} \tag{3}$$

with K_j being the inhibition constant. Factors of other forms may be used as well. The general expression for a specific reaction rate as a function of its factors is

$$q_i = q_i^{\max} \prod_{j=1}^{N_{\text{factors}}} \varphi_j \quad [M_M M_p^{-1} T^{-1}] \tag{4}$$

As each factor produces a value in the range of 0–1, Eq. 4 will produce for the specific growth rate q_i a value that is a fraction of the maximum specific growth rate q_i^{max}. The net rate (r_n) for a species n, either solute or particulate, results from the sum of the rates of all the reactions in which the species is involved, each multiplied by a yield coefficient specific of that reaction (Y_{nm}^i) and a sign factor (γ_{in}). The yield coefficient is always positive and has units of mass of species n per mass of the reference of the reaction i, species m. The sign factor γ_{in} has value +1 or −1 if the species n is, respectively, produced or consumed in reaction i. For a species n involved in a number N of reactions, the net rate R_n becomes

$$R_n = \frac{dC_n}{dt} = \sum_{i=1}^{N} \gamma_{in} Y_{nm}^i q_i C_p \quad [M_n L^{-3} T^{-1}] \tag{5}$$

This form for bioconversion rates is suitable for a description of bioprocesses that uses stoichiometric tables, a concept commonly used to describe biological processes in engineering applications. A typical example is the Activated Sludge Model No. 2 (Gujer and Larsen, 1995). The case study presented later in this article also uses a stoichiometry table to describe reaction rates of the bioprocesses involved (Table 1).

To allow for including structured biomass into the IbM, a *pDocument type* is also defined. Each pDocument type groups a number of particulate species and determines the particulates that will constitute individual biomass particles. For example, a pDocument type called 'heterotrophic bacteria' may be defined as being composed by two particulate species – 'heterotrophic active mass' and 'inert biomass'. Any particle ('agent') of the pDocument type 'heterotrophic bacteria' will have a biomass composition containing these particulate species. The dynamics of the biomass composition of such an organ-

Table 1. Stoichiometric table for the model described the case study.

	Solute species		Particulate species					
Reaction	Substrate C_S	Oxygen C_O	H-PHB $C_{H\text{-}PHB}$	PHB C_{PHB}	H-EPS $C_{H\text{-}EPS}$	EPS C_{EPS}	Inert C_I	Rate
Carbon source uptake by H-PHB (feast)	−1	$-(1-Y_{PS})$		Y_{PS}				$q_S^{max}\cdot\varphi_{M,S}\cdot\varphi_{M,O}\cdot\varphi_{I,f_{PHB}}\cdot C_{H\text{-}PHB}$
Growth H-PHB (feast)		$-\left(\frac{Y_{PS}}{Y_{HS}}-1\right)$	1	$-\frac{Y_{PS}}{Y_{HS}}$				$\mu^{max}\cdot\varphi_{M,S}\cdot\varphi^{*}_{M,O}\cdot X_{H\text{-}PHB}$
Decay H-PHB	0.6		−1				0.4	$b_{decay}\cdot C_{H\text{-}PHB}$
PHB consumption H-PHB (famine)		$-(1-Y_{HP})$	Y_{HP}	−1				$k_{PHB}\cdot\phi_{I,S}\cdot\phi_{M,O}\cdot C_{PHB}$
Carbon source uptake by H-EPS (feast)	−1	$-(1-Y_{PS})$				Y_{PS}		$q_S^{max}\cdot j_{M,S}\cdot j_{M,O}\cdot j_{I,f_{EPS}}\cdot c_{H\text{-}EPS}$
Growth H-EPS (feast)		$-\left(\frac{Y_{PS}}{Y_{HS}}-1\right)$			1	$-\frac{Y_{PS}}{Y_{HS}}$		$\mu^{max}\cdot\varphi_{M,S}\cdot\varphi^{*}_{M,O}\cdot X_{H\text{-}EPS}$
Decay H-EPS	0.6				−1		0.4	$b_{decay}\cdot C_{H\text{-}EPS}$

Rows represent the reactions and columns represent the species involved, both solute and particulate. Entries in the table provide the value of the yield coefficient (Y) for each combination of reaction and species multiplied by the sign factor (γ), which has value +1 if the species is produced in the reaction and value −1 if it is consumed. Empty entries represent value 0. Net rates for each of the species are obtained from the sum of the reaction rates, each multiplied by its respective entries in the matrix, as described in a generic way in Eq. 5. For example, the net rate of substrate conversion, Rs, which is consumed by H-PHB and H-EPS but produced in the decay processes, is given by $R_S = -1\times q_S^{max}\cdot\varphi_{M,S}\cdot\varphi_{M,O}\cdot\varphi_{1,f_{PHB}}\cdot C_{H\text{-}PHB} + 0.6\times b_{decay}\cdot C_{H\text{-}PHB} - 1\times q_S^{max}\cdot\varphi_{M,S}\cdot\varphi_{M,O}\cdot\varphi_{1,f_{EPS}}\cdot C_{H\text{-}EPS} + 0.6\times b_{decay}\cdot C_{H\text{-}PHB}$. The entries have values expressed in mass of oxygen or (chemical oxygen demand) COD and the sum of the entries in each row is 0, which ensures conservation of mass. For example, when 1 g_{COD} of H-PHB decays, 0.6 g_{COD} of substrate and 0.4 g_{COD} of inert mass are produced. Where $\varphi_{M,S}=\frac{C_S}{C_S+K_S}$; $\varphi_{1,S}=\frac{K_S}{X_S+K_S}$; $\varphi_{1,f_{PHB}}=\frac{K_P}{f_{PHB}+K_P}$; $f_{PHB}=\frac{C_{PHB}}{C_{H\text{-}PHB}}$; $\varphi_{1,f_{EPS}}=\frac{K_P}{f_{EPS}+K_P}$; $f_{EPS}=\frac{C_{EPS}}{C_{H\text{-}EPS}}$; $\varphi_{M,O}=\frac{C_O}{C_O+K_O}$; $\varphi^{*}_{M,O}=\frac{C_O}{C_O+K^{*}_O}$.

ism would be dictated by the reactions in which the two particulate species are involved.

Individual-based model and mass balances for particulate species. The representation of biomass using individual agents constitutes the smallest scale of a multiscale representation of the biofilm system used in this framework, which describes the biofilm at the (A) individual scale, the (B) biofilm scale and the (C) system scale, as illustrated in Fig. 1. Agents are entities that have dynamic biomass composition and location in space, and behave according to a set of rules that mimic the processes carried out by a bacterial cell. Agents grow by uptake of nutrients, produce and excrete metabolites such as EPS, and divide once a critical size is reached producing an offspring agent. Agents are best viewed as biomass particles rather than individual cells. The agents move if shoved by a neighbouring agent or by being repelled by the solid surface. The behaviour rules of agents are illustrated in Fig. 1A. The biomass particles (called 'agents') are spherical (in case of 3D simulations) or cylindrical (in case of 2D simulations) compartments, with variable composition and location in space and where bioconversions take place. Depending on the value chosen for the maximum particle radius ($R_{division}$), biomass particles can represent either a single cell or a cluster of cells of the same species. This abstraction is a numerical convenience to allow the description of larger scale systems without the added computational burden of using an increased number of agents. Effectively, it allows setting the resolution of the field of particulate matter in the simulation according to each particular application. The mass of each particulate species (n) that is part of the composition of a biomass agent changes in time according to the kinetic equation

$$\frac{dM_n}{dt}=\sum_{i=1}^{N}\gamma_{in}Y_{ms}q_iM_p \quad [M_n\,\text{particle}^{-1}T^{-1}] \tag{6}$$

which is Eq. 5 written in terms of mass per particle. M_n and M_p is the mass of particulate species n and particulate species m (the species that mediates reaction i), respectively, in that particular agent. As the masses of the composing particles change as a result of the bioconversions occurring, also the size of the agent will change. The volume of the agent is obtained from the sum of the masses of all the composing particulate species divided by their respective specific mass (ρ_m):

$$V_{particle}=\sum_{m=1}^{N_{particulates}}\frac{M_m}{r_m} \quad [L^3] \tag{7}$$

$N_{particulates}$ is the number of particulate species composing the agent, as defined by its pDocument type. The specific mass of a particulate species sets the maximum mass of that species per particle volume. Equation 7 is fundamental for the IbM, as it is responsible for the important changes in the size of the agents that occur in the course of the simulations. Such changes include not only growth of an agent from the production of active biomass but also size reduction of an agent when its mass decreases through processes such as biomass decay. The radius of the agent particle is defined by

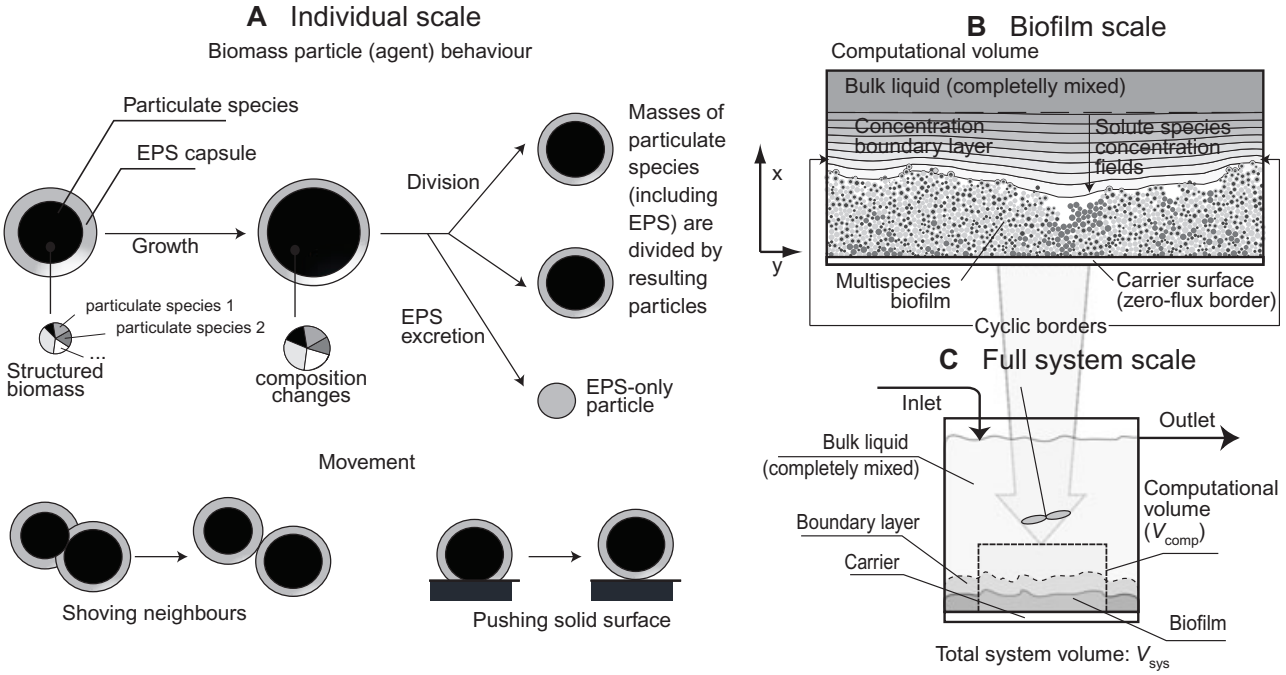

Fig. 1. Three scales considered in multidimensional biofilm modelling. Actions occurring at the individual scale (A) define dynamics at the community level (B, biofilm scale) which, in turn, define overall conversions occurring at the full system scale (C). The bulk liquid is modelled as a completely mixed container. The total area of the biofilm carrier material in the system is $A_{carrier}$. The computational domain represents a fraction of the total system, a subvolume of volume V_{comp}.

$$R_{particle} = \begin{cases} \sqrt[3]{\dfrac{3V_{particle}}{4\pi}} & \text{if 3D} \\ \sqrt{\dfrac{V_{particle}}{2\pi L_z}} & \text{if 2D} \end{cases} \quad [L] \tag{8}$$

and depends on the dimensionality of the simulation being carried out. For 3D simulations, biomass particles are spheres, whereas (for mass conservation reasons) 2D simulations particles are cylinders with a height L_z.

Reproduction of an agent occurs by division when the radius of a particle reaches $R_{division}$. The masses of all particulate species contained in the dividing agent are then redistributed between the two resulting agents. Specific routines are attributed to EPS, represented as a capsule surrounding the remaining particulate substances in a biomass particle as shown in Fig. 1A. EPS excretion occurs when the mass fraction of EPS relative to total agent mass reaches a critical value $f_{EPS,excretion}$. The excreted mass generates an EPS-only particle.

Detachment and other biomass losses. Mechanical stresses effective on the entire surface of the biofilm, such as erosion caused by shear forces (Characklis, 1990), are here modelled using a continuous detachment speed function F_{det}. This method, which is a multidimensional extension of the method used in the 1D model of Wanner and Gujer (Wanner and Gujer, 1986) is described by

$$\frac{d\boldsymbol{x}}{dt} = -F_{det}(\boldsymbol{x})\boldsymbol{n}(\boldsymbol{x}) \quad [LT^{-1}] \tag{9}$$

where $\boldsymbol{x}$ is the location of a point on the biofilm interface, $F_{det}(\boldsymbol{x})$ is the value of the detachment speed function at that point and $\boldsymbol{n}(\boldsymbol{x})$ is the vector normal to the biofilm surface at point $\boldsymbol{x}$. In line with the multidimensional characteristics of this modelling framework, Eq. 9 is valid in 2D, where $\boldsymbol{x}$ is defined by coordinates (x, y), or 3D, where $\boldsymbol{x}$ is defined by coordinates (x, y, z). The method used is flexible to allow F_{det} to take several forms, including expressions where local values of $F_{det}(\boldsymbol{x})$ are dependent on state variables such as local biofilm density or the local concentration of detachment-inducing chemical species. Integration of the detachment routines with the multidimensional IbM was carried out by using a novel application of the level set method. The details of this integration are not in the scope of the present article and will be reported in a forthcoming article. It is noteworthy, however, that this method allows discrete detachment events that derive from random instabilities in the surface, i.e. biomass sloughing, to be implicitly derived from the simulations. Erosion and sloughing are this way modelled using the same mechanism, producing results equivalent to those obtained from a previous implementation of fluid-induced detachment in a 2D biofilm model (Picioreanu *et al.*, 2001).

Other biomass losses by processes such as decay cause a reduction of the size of the biomass agents. This is a direct consequence of the application of Eq. 7, which translates the mass of an agent composition into its volume. 1D models (Wanner and Gujer, 1986) also implement the retreat of the biofilm front (i.e. a net reduction of the biofilm volume) in conditions where biomass losses occur from processes such as decay of EPS or inactivation of the bacterial biomass (Horn *et al*., 2001). Similarly, the IbM was extended here to include net reduction of the biofilm volume by bringing the biomass agents together whenever volume reduction occurs. If the net change in agent volume is negative at any given iteration (i.e. a biomass particle shrinks), the agent will pull the neighbouring agents towards itself by a distance that is equal to the reduction in its radius.

Mass balances of solutes in the biofilm. If the effects of solute transport by fluid convection can be neglected (such conditions are presented in Eberl *et al*., 2000; Picioreanu *et al*., 2000b), the dynamics of the concentration of a solute S is defined in its general form by a diffusion-reaction equation

$$\frac{\partial C_S}{\partial t} = \nabla \cdot (D_S(\nabla \cdot C_S)) + r_S \quad [M_S L^{-3} T^{-1}] \tag{10}$$

where the nabla (∇) operator is the gradient of a function in Cartesian coordinates, a representation that is valid for both 2D and 3D. In Eq. 10, the value for the diffusivity of the solute (D_S) can be variable in space to account for local differences in mass transfer resistance. This may be relevant for modelling biofilm systems, as the resistance to the diffusion of solutes in the biofilm matrix may be higher than in the bulk liquid. Moreover, the local values of diffusivities in the biofilm may be a function of the biomass composition (Beuling *et al*., 1998, 2000).

The computation of solute concentration fields is decoupled from biomass dynamics. This decoupling is an approach originally developed for cellular-automata (CA) biofilm models (Picioreanu *et al*., 1998, 1999) and later applied to individual-based modelling (Kreft *et al*., 2001; Picioreanu *et al*., 2004). The solute and biomass dynamics are calculated sequentially based on the rationale that time-scale of solute transport and reaction is orders of magnitude shorter than that of biomass spreading (Picioreanu *et al*., 2000b). As a consequence, the diffusion-reaction of solutes can be considered to reach a steady state between each biomass spreading iteration. Thus, Eq. 10 may be simplified to:

$$\nabla \cdot (D_S(\nabla \cdot C_S)) + r_S = 0 \quad \text{in the biofilm and concentration boundary layer} \tag{11}$$

$$C_S = C_S^{\text{bulk}} \quad \text{outside the concentration boundary layer} \tag{12}$$

Outside the boundary layer, the liquid is assumed to be completely mixed as shown in Fig. 1B and C.

For the computational volume defined as shown in Fig. 1B, where the bottom side corresponds to the solid carrier surface, the bottom border is a zero-flux boundary

$$\frac{\partial C_S}{\partial x} = 0 \quad \text{for } x = 0 \tag{13}$$

At the top boundary, the concentrations in the bulk liquid are set as in Eq. 12, and the lateral borders of the computational volume (in the y direction, for 2D, or in the y and z direction, for 3D) are periodic.

Bulk concentration of solutes. The framework allows bulk concentration of solutes to be either imposed or computed from mass balances to the system. Each solute species defined in the system may have a different behaviour for the value of its bulk concentration. Imposed bulk concentrations may be *constant*, in which case the bulk liquid is assumed to be an infinite and constant supply of the solute throughout the whole simulation, or *intermittent*, where the bulk concentration is changed to impose a feast and famine cycle. In the latter, stepwise changes are produced to cyclically vary the bulk concentration of a solute (C_S^{bulk}) between a value for feast concentration (C_S^{feast}) and a famine concentration (C_S^{fam}):

$$\begin{aligned} C_S^{\text{bulk}} &= C_S^{\text{fam}} \quad \textit{for famine period} \\ C_S^{\text{bulk}} &= C_S^{\text{feast}} \quad \textit{for feast period} \end{aligned} \quad [M_S L^{-3}] \tag{14}$$

The use of this type of behaviour is illustrated in the case study section in the application of the feast/famine feeding regime.

Bulk concentrations may also be computed from mass balances to the system. In this case, the computational volume V_{comp} is a subregion of the full system, volume V_{sys}. This is illustrated in Fig. 1C. The dynamics of the bulk concentration of a solute species S are then expressed by

$$\frac{\mathrm{d}C_S^{\text{bulk}}}{\mathrm{d}t} = Q \cdot C_S^{\text{in}} - Q \cdot C_S^{\text{bulk}} + R(C_S^{\text{bulk}}) \tag{15}$$

$$\text{where } R(C_S^{\text{bulk}}) = \frac{A_{\text{carrier}}}{L_y L_z V_{\text{sys}}} \int_{V_{\text{comp}}} r_S(x)\mathrm{d}V \tag{16}$$

In the dynamic behaviour, the net rates of consumption or production of the solutes in the computational volume (described by the integral in Eq. 16) are used to define the overall rate in the system, $R(C_S^{\text{bulk}})$. The scaling to the full reactor scale is performed by the ratio between the substrate surface area in the whole system (A_{carrier}) and the substrate surface area in the computational volume (Ly, Lz).

Numeric implementation of the framework

The processes involved in biofilm formation are implemented sequentially to compose a *simulation cycle*, which

is repeatedly executed in the course of a simulation to follow the biofilm development in time. In the simulation cycle, the operations concerning biomass growth and spreading are executed first and followed by the updating of the solute concentrations. The last step is the update of the simulation time and the cycle is then restarted. The sequence of steps that composes the simulation cycle is the following:

1. Determination of the time step, Δt, for the present iteration at time t.
- Biomass growth and spreading operations.
  2. Growth of every biomass agent, with eventual agent division if its radius is greater than $R_{division}$ and EPS excretion if its fraction of EPS is greater than $f_{EPS,excression}$.
  3. The spreading cycle, in which the biofilm front advances.
  4. Biomass detachment, including erosion and sloughing.
- Updating the solute concentration fields.
  5. The update of the bulk concentration of solutes, performing global mass balances for solutes with dynamic behaviour.
  6. Update of the spatial concentration fields of solutes to steady state.
7. Advance the simulation time to $t = t + \Delta t$ and restart the simulation cycle from (1).

This simulation cycle extends previously proposed cycles (Picioreanu *et al*., 2001, 2004) by using a variable time step (Δt). The variable time step is essential to permit use of the framework for the modelling of diverse biofilm systems. The iteration time step must be adaptable to guarantee the numeric stability of all steps performed in the simulation cycle. The algorithm used for determination of Δt applies constraints defined at the three scales in which the biofilm system is described. Constraint Δt_1, concerning the individual scale, imposes that no biomass agent should more than double its size at any given iteration step. Application of this constraint is necessary to ensure that no agent exists with a radius greater than $R_{division}$. Constraint Δt_2, concerning the biofilm scale, imposes that the total biofilm volume should not grow more than a fraction of its volume, f_V, at any iteration. This constraint is necessary to guaranty the stability of step (3), the spreading cycle. Constraint Δt_3 is relative to the global mass balances and guaranties stability of the numeric method used in the determination of the bulk concentrations of solute species. The iteration time step selected at each iteration is the minimum among these three values:

$$\Delta t = \min(\Delta t_1, \Delta t_2, \Delta t_3) \quad [T] \tag{17}$$

The value of Δt is recomputed at the beginning of each iteration.

Growth of agents, as well as division and EPS excretion, results in the overlapping of neighbouring agents. A spreading cycle is then used to release this overlap in the course of which neighbouring agents shove each other until all overlap is undone. This iterative spreading process, an important component of the IbM, was described in detail previously (Kreft *et al*., 1998).

Solving efficiently the diffusion-reaction Eq. 11 for all the solute species involved in the system requires the use of advanced numerical techniques. Here, a non-linear multigrid solver (Press *et al*., 1997), applied previously for biofilm modelling (Picioreanu *et al*., 2004), was extended to allow diverse mass-transfer boundary layer shapes to be defined. Multigrid solvers are very efficient, but the computation of the solute concentration fields still constitutes one of the most demanding procedures of the simulation. This procedure is typically the longest step of the computational cycle at the initial stages of a simulation, when the number of biomass agents in the system is still reduced. For relatively large numbers of agents in the system (in the order of the tens of thousands) computing the concentration fields usually becomes negligible in comparison with the spreading cycle.

Using the framework

The framework for biofilm modelling described here was implemented into a computer program code written in the Java programming language. The program, in the form of a library of compiled Java classes, is available for download from our website (Xavier *et al*., 2004a) and may be readily used to create 2D and 3D biofilms models with multiple bacterial and solute species. The website includes also a brief guide and how to use the *Eclipse* Java editor (freely obtainable from http://www.eclipse.org) to start developing models. Use of the program in the present form, however, requires knowledge of the Java programming language. To facilitate all readers to experiment the program, an interactive demonstration was set up. This demonstration is accessible at http://www.biofilms.bt.tudelft.nl/frameworkMaterial/monospecies2d.html and shows a monospecies biofilm model with a single solute species (oxygen) present. Model parameters influencing the properties of the microorganims and three environment properties (bulk oxygen concentration, boundary layer thickness and detachment forces) may be changed in the course of the simulation and their effect in the biofilm developing observed in real time.

The program code used to implement the present model framework was created entirely following object-oriented design techniques. The choice of Java as opposed to the C++ programming language, as used in previous implementations of biofilm models from our

group, was justified by the conveniences provided by this recent but well-established technology. Advantages of Java include platform independence, i.e. compiled Java programs are fully portable to any platform for which a Java implementation exists, such as UNIX systems, GNU/Linux, Microsoft Windows and MacOS X. The framework was programmed with special emphasis on the structure of class hierarchies and to provide complete documentation according to the Javadoc standard. The program provides functionality for output of simulation results such as time course of solute and particulates concentration fields, location of biomass particles, global solute conversion rates, biomass detachment rates, etc. Outputs are generated as tables in ASCII text files, which can be easily used with applications such as MATLAB (the Mathworks) or spread sheeting programs (e.g. Microsoft Excel) for further analysis. The program also produces output for rendering of 3D ray-traced images of the simulated biofilm using the POV-Ray program (freely available from http://www.povray.org).

Formulation of biofilm models using the framework. Following is the sequence of steps necessary to create a biofilm model using the framework:

1. Choosing the system dimensionality – either 2D or 3D – and the scale (in length units) of the computational volume.
2. Definition of the maximum radius of biomass particles ($R_{division}$) and the grid resolution for the solute concentration fields.
3. Definition of the solute and particulate species involved in the system, as well as the reactions taking place. This is straightforward if the reactions are described using a stoichiometric table. A value for the molecular diffusivity of each solute species in the system must be set at this point, as well as the behaviour of the corresponding bulk concentration (either *constant*, *intermittent* or *computed from mass balances*), and a value for the specific mass of each particulate species. The *pDocument type*, which group the particulate species allowed for each agent, must be defined together with an initial composition for the inoculating particles.
4. Definition of the expressions for reactions rates and association of the reactions with each species involved using the yield coefficients.
5. Definition of the detachment speed function, F_{det}, which may either be chosen from a library of predefined detachment functions provided with the framework or created by the user.
6. The boundary layer must also be defined, either taken from a supplied set of predefined boundary layer types or created by the user.
7. Definition of the criterion for ending the simulation.

Case study – competition between internal storage compound producing and EPS producing bacteria in biofilms

The case study presented here is a biofilm model where the competition between two bacterial species is analysed. The biofilm system chosen uses a structured representation of biomass that includes EPS and internal storage compounds. The relative importance of these compounds in the presence of different feeding regimes is analysed.

Production of biopolymers by bacteria

In the presence of surplus source of carbon and energy some microorganisms produce intracellular storage polymers. Other microorganisms, in turn, excrete large amounts of polysaccharides to the medium. The synthesis of both such type of compounds is promoted when growth is restricted by the availability of essential nutrients other than the carbon source. Polyhydrohyalkanoates (PHA), glycogen and lipids are examples of intracellular storage compounds that may constitute a reserve of carbon and energy (Anderson and Wynn, 2001) and can be used to survive periods of famine. In wastewater treatment processes, particularly in sequencing batch processes, microorganisms are subject to intermittent feeding regimes and variation in the presence of an electron acceptor. It is observed that accumulating internal storage compounds such as polyhydroxybutyrate (PHB), the most common PHA, occurs as a response to these 'feast and famine' regimes (Van Loosdrecht *et al.*, 1997). Figure 2 shows a photograph of bacterial cells containing granules of PHB. The importance of internal storage polymers in such bioprocesses suggests the dynamics of their formation and consumption should be included in bioprocess models (Van Loosdrecht and Heijnen, 2002). Furthermore, the production of PHA from waste using mixed cultures is a very promising technology that exploits this

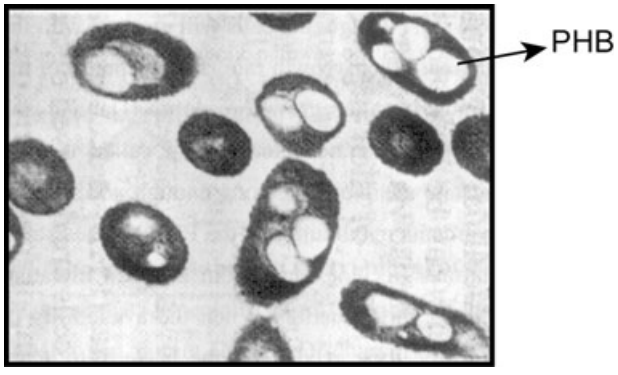

Fig. 2. Photograph of bacterial cells with PHB granules, reproduced from the study by Beun (2001).

natural ability of microorganims to produce internal storage polymers (Reis *et al*., 2003).

Microorganisms that are able to quickly store available substrate as PHB and consume the storage when substrate is depleted in order to achieve a more balanced growth rate have a strong competitive advantage over organisms without this storage capability (Van Loosdrecht and Heijnen, 2002). Both production of internal storage compounds and EPS constitute cases where biomass composition is dynamic and therefore require modelling approaches that use a structured description of the biomass.

Model description

In this case study, two microbial types are defined: a heterotrophic PHB-accumulating strategist, denoted as H-PHB, and a heterotrophic EPS producer, H-EPS. Competition between the two species in a hypothetical system is analysed here in respect with two feeding regimes:

- Constant feeding regime: the bulk concentration of carbon source is constant in time ($C_S^{bulk} = 0.1\ g_{COD\text{-}S}\ l^{-1}$).
- Feast/famine regime: 24 h cycles of substrate feeding (feast), with a duration of 4 h ($C_S^{feast} = 0.6$ gCOD-S l-1), and substrate absence (famine), with a duration of 20 h ($C_S^{fam} = 0$).

Bulk concentrations of the carbon source in the feast period are defined so that the total amount of substrate fed per day equals to that of the constant feeding case. Organic carbon quantities are represented in terms of gram of chemical oxygen demand (COD), a usual procedure in wastewater treatment processes. The bulk concentration of oxygen was kept constant at $4\,mg_{O_2}\,l^{-1}$.

A simplification of a kinetic model proposed for activated sludge processes by Van Loosdrecht and Heijnen (2002) is used here to describe the heterotrophic PHB accumulating organism. In order to compare on a reasonable basis the effect of the two metabolic strategies on the biofilm structure, maximum carbon source uptake rates are set equal for both microbial species as well as their growth kinetics. Production of polymeric substances, either PHB or EPS, when the system is not carbon source limited also has the same kinetics for both species. Stoichiometry of the reactions involved is described using a stoichiometric table, shown in Table 1. The parameters used for the simulations and their values are listed in Table 2. In these conditions, rates for polysaccharide (the index 'P' when used represents either PHB or EPS) production results from the difference between the actual carbon source uptake rate and the growth rate of the heterotrophic species (the index 'H', here representing either H-PHB or H-EPS) that produces it

$$R_p = Y_{SP} q_S^{max} \cdot \varphi_{M,O} \cdot C_H - \frac{Y_{PS}}{Y_{HS}} m^{max} \cdot \varphi_{M,O}^{*} \cdot C_H$$
$$= Y_{PS} \cdot q_S^{max} \cdot (\varphi_{M,O} - \varphi_{M,O}^{*}) \cdot C_H \quad [M_P L^{-3} T^{-1}] \qquad (18)$$

Two different saturation (Monod type) factors, $\phi_{M,O}$ and $\varphi_{M,O}^{*}$, are used here to model the dynamics of PHB accumulation in the feast period. When carbon source is in excess, organisms increase the substrate uptake rate but balance their growth rate and the excess results in the production polymeric substances. When carbon source is removed, H-PHB organisms are able to consume their internal storage for growth and maintenance. PHB consumption has been observed (Beun *et al*., 2002) to have first-order kinetics on the fraction of PHB (f_{PHB}). Here it will be assumed that organisms do not consume the EPS. The comparison between the production of PHB by H-PHB organisms, which are able to consume their PHB storage, and EPS by H-EPS organisms is illustrated in Fig. 3A. From Eq. 18 it results that the rate of polymer (either PHB or EPS) production is low when either oxygen concentration is very low or when no oxygen limitation exits, and the rate has a maximum when $C_O = \sqrt{K_O \cdot K_O^{*}}$. This trend is illustrated in the plot shown in Fig. 3B.

As kinetics and stoichiometry for PHB and EPS producers are set to be the same, both species would be equally competitive in continuously fed suspended culture when no carbon sources limitations exist. When carbon source concentration is limiting, PHB producers would have an advantage by recycling any PHB produced and using it for growth. In biofilms, however, spatial structure plays an important role. As EPS is less dense than PHB, EPS-producers create a larger volume for the same mass of polymer produced. As it will be shown later, this can constitute a competitive advantage for H-EPS when oxygen is growth limiting, such as the case where feeding of carbon source is constant.

Results of simulations

The biofilm model described above was implemented using the framework program. 2D and 3D simulations were carried out for both the continuous feeding and the feast/famine cases. Figure 4 shows time-course of the particulate species throughout the 2D simulations. Figure 5 shows the legend for interpretation of the 2D biofilm structure for Figs 6 and 7. Figure 8 shows biofilm structures obtained from 3D simulations.

Time-course of particulates species composing the biofilm from 2D simulations (Fig. 4A) shows that after 1500 h, H-EPS organisms become predominant over H-PHB. This is observable from the evolution of biofilm structures, pictured in Fig. 6 at 1 h, 103 h, 238 h and 1500 h, where H-EPS organisms are shown in red and H-PHB organisms are shown in a colour ranging from blue to yellow, depend-

Table 2. Parameters used for simulations.

Parameters	Description	Value	Units	Notes/references
Solute species				
C_S^{bulk}	Bulk substrate concentration	0.1	$g_{COD\text{-}S}\ l^{-1}$	
	in continuous feeding	0.6	$g_{COD\text{-}S}\ l^{-1}$	
	in feast phase			
C_O^{bulk}	Bulk concentration of oxygen	0.004	$g_O\ l^{-1}$	
D_S	Diffusivity of substrate	1×10^{-4}	$m^2\ day^{-1}$	Rittmann and colleagues (2004)
D_O	Diffusivity of oxygen	2×10^{-4}	$m^2\ day^{-1}$	Rittmann and colleagues (2004)
Particulate species				
ρ_H	Specific mass of active biomass (H-EPS or H-PHB)	200	$g_{COD\text{-}H}\ l^{-1}$ of particle	
ρ_{PHB}	Specific mass of PHB	1000	$g_{COD\text{-}PHB}\ l^{-1}$ of particle	
ρ_{EPS}	Specific mass of EPS	33.3	$g_{COD\text{-}EPS}\ l^{-1}$ of particle	Six times less dense than activebiomass Horn and colleagues (2001)
ρ_I	Specific mass of inerts	200	$g_{COD\text{-}I}\ l^{-1}$ of particle	Same as active biomass Horn and colleagues (2001)
Yield coefficients				
Y_{HS}	Yield of active mass (H-EPS or H-PHB) on carbon source	0.495	$g_{COD\text{-}H}\ g_{COD\text{-}S}^{-1}$	Beun and colleagues (2002)
Y_{PS}	Yield of polymers (EPS or PHB) on carbon source	0.667	$g_{COD\text{-}P}\ g_{COD\text{-}S}^{-1}$	Beun and colleagues (2002)
Y_{HP}	Yield of H-PHB relative to PHB consumed	0.668	$g_{COD\text{-}H\text{-}PHB}\ g_{COD\text{-}PHB}^{-1}$	Beun and colleagues (2002)
Rate parameters				
q_S^{max}	Maximum specific substrate uptake rate of microorganisms	0.952	$g_{COD\text{-}S}\ g_{COD\text{-}H}^{-1}\ h^{-1}$	Beun and colleagues (2002)
μ^{max}	Maximum specific growth rate of microorganisms	0.47	$g_{COD\text{-}H}\ g_{COD\text{-}H}^{-1}\ h^{-1}$	From $\mu^{max} = q_s^{max} \cdot Y_{SX}$
K_S	Saturation constant for substrate	0.004	$g_{COD\text{-}S}\ l^{-1}$	Rittmann and colleagues (2004)
K_O	Saturation constant for oxygen	3.50×10^{-4}	$g_O\ l^{-1}$	Rittmann and colleagues (2004)
K_O*	Saturation constant for oxygen*	7.00×10^{-4}	$g_O\ l^{-1}$	Assumed
K_P	Inhibition constant for polymer (EPS or PHB) fraction	1	$g_{COD\text{-}P}\ g_{COD\text{-}H}^{-1}$	Assumed
b_{decay}	Decay rate coefficient	3.3×10^{-3}	$g_{COD\text{-}H}\ g_{COD\text{-}H}^{-1}\ h^{-1}$	Rittmann and colleagues (2004)
k_{PHB}	PHB degradation rate coefficient	0.15	$g_{COD\text{-}PHB}\ g_{COD\text{-}PHB}^{-1}\ h^{-1}$	Beun and colleagues (2002)
k_{det}	Detachment speed constant	3×10^{-3}	$g\ L^{-1}\ \mu m^{-1}\ h^{-1}$	
Computation parameters				
System size		1000×1000	μm^2	
$R_{division}$	Maximum particle radius	8	μm	
f_V	Fraction of volume for constraint Δt_2	0.1		
$f_{EPS,excretion}$	Critical volume fraction of EPS	0.7		
L_C	Boundary layer thickness	100	μm	
Δx	Grid element size (for solute concentrations)	30.3	μm	

Index 'H' refers to active biomass of either H-EPS or H-PHB, index 'P' refers to biopolymers, either EPS or PHB.

ing on the fraction of PHB in their composition. The observed advantage of H-EPS organism is attributed to the fact that, thanks to the extra volume of EPS produced, EPS producers spread more rapidly than PHB producers. Being pushed upward and taking advantage of the higher concentrations of oxygen in the top layers of the biofilm provides a competitive edge to EPS producing organisms. In Fig. 4A it is observable that PHB is accumulated but is not consumed in the course of the simulation, as its consumption is inhibited by the constant presence of carbon source. It is also noteworthy the occurrence of a sloughing event at 1100 h (see doted line in Fig. 4A). This occurrence resulted in the loss of a biomass cluster mainly composed by PHB producing organisms and the consequent decreased of the fraction of H-PHB biomass in the biofilm, which reached values of less than 50% of its value prior to the sloughing event. This further contributed to the advantage of H-EPS organisms, the amount of which increased immediately after the occurrence of this sloughing event.

This competition is reversed in feast/famine regimes (2D simulation results are shown in Figs 4B and 7). Time-course of the biomass components (Fig. 4B) shows oscillatory behaviour for active biomass of both H-EPS and

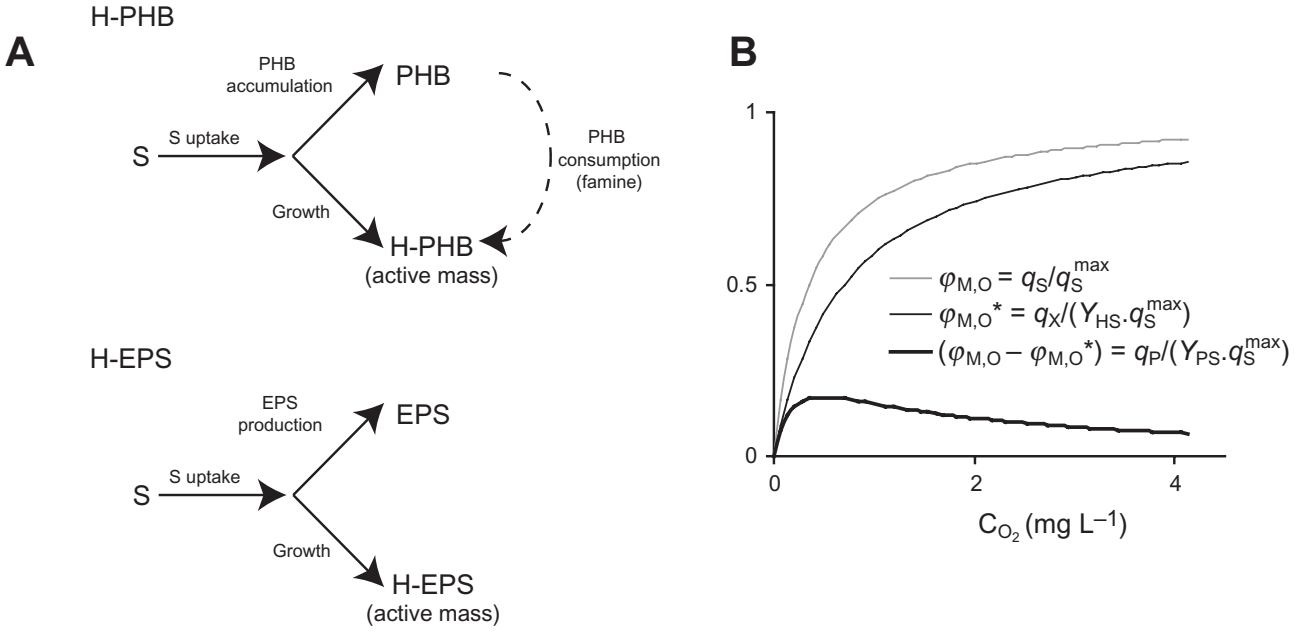

Fig. 3. A. The processes involved in the substrate uptake and biomass production by H-PHB (PHB producers organisms, top scheme) and H-EPS (EPS producers, bottom scheme). The polymer (either PHB or EPS) formation rate results from the difference between S-uptake rate and the growth rate. In addition, H-PHB organisms have the ability to consume their PHB storage when external carbon source is low.
B. Function defining specific polymer (either PHB or EPS) production rate in terms of consumed substrate ($-q_P/Y_{PS}$) as a function of the oxygen concentration. Values are shown normalized by the maximum specific substrate uptake rate (q). q_P/Y_{PS} is the difference between specific substrate taken up (q_S) and that used for growth (q_X/Y_{HS}). In this kinetic description polymer production is low for both low and high values of C_O, having a maximum when $C_O =$. If $K_o^* = 2K_o$ a maximum at $q_P/Y_{PS}q$ ~0.17 occurs.

H-PHB in the course of simulations, increasing during the feast period (when external substrate concentration is $C_S^{bulk} = 0.6\ g_{COD\text{-}S}\ l^{-1}$) and decreasing in the famine period (when substrate concentration is 0). This is pictured in the detail in Fig. 4C (showing the oscillatory feast/famine pattern of C_S^{bulk} between 215 and 265 h) and Fig. 4D (showing the evolution of particulate species in the same period). Losses of active mass of both species in the famine period result from decay processes and detachment. However, the net growth of H-PHB organism is positive throughout most of the simulation, whereas the net growth of H-EPS is mostly negative. This is explained by the fact that the use of PHB reserves allows H-PHB organisms to suffer less the effects of the absence of external substrate in famine periods than H-EPS organisms. The total quantity of PHB in the biofilm oscillates throughout the simulation, increasing as it is stored by H-PHB in the feast phase and decreasing as it is consumed to allow growth of H-PHB in the famine phase. Growth of H-PHB organisms in the famine period is slower than in the feast period. However, it is not oxygen-limited. This fact is observable from the computed oxygen concentration fields (shown for the biofilm at 868 h in Fig. 7B), showing that oxygen penetrates well into the biofilm in the famine phase when compared with the feast phase (shown for the biofilm at 888 h in Fig. 7C).

Although the averaged bulk concentration of substrate is the same in both the continuous feeding case and the feast/famine case, a much thinner biofilm is obtained in the latter. This is observable from a comparison between the structure of biofilm at the end of the simulation from the continuous case (shown in Fig. 6D) and the feast/famine case (shown in Fig. 7D). This lower biofilm accumulation is both a consequence of the lower EPS content (a low density particulate species) and of the fact that carbon source uptake rate in the feast period is oxygen-limited and the organisms do not take full advantage of the high concentration of carbon source in the feast period, producing in total less biofilm mass.

It is clear from the 2D simulation results that H-EPS organisms have the competitive advantage in the constant feeding case, whereas in the feast/famine case this advantage is reversed and H-PHB predominate. Animations of the 2D simulations may be obtained from the support website (Xavier *et al*., 2004a). Simulations in 3D (shown in Fig. 8) were also carried out, yielding the same qualitative results.

Discussion and conclusions

The framework presented here provides mathematical and mechanistic concepts for the implementation of time-

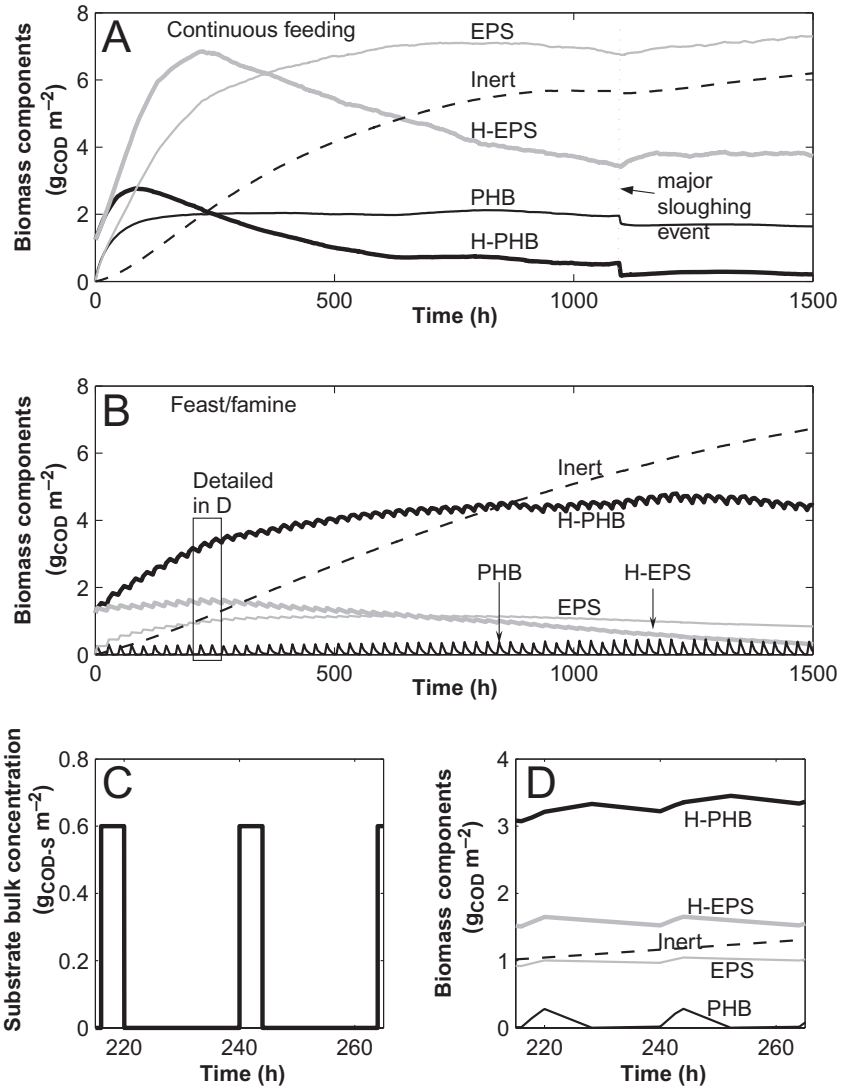

Fig. 4. A and B. Time-course of particulate species composing the biomass in the biofilm from 2D simulations of 1500 h of biofilm development, according to the model presented in the case study.
A. Continuous feeding.
B. Feast/famine case.
C. Variation of the substratum bulk concentration in the feast/famine case, shown for the time period of 215–265 h.
D. Detailed plot of the evolution of the biofilm biomass composition for the period of 215–265 h. See text for details.

dependent and spatially multidimensional (2D or 3D) models of biofilms based on principles of conservation of mass, as well as the implementation of these concepts into a computer program.

A central characteristic of the framework is the discrete biomass representation using IbM, which is a bottom-up approach where the rules for the behaviour of the individual agents (biomass particles here) composing elements are provided and the dynamics of a multispecies biofilm emerges from the simulations. The IbM has similarities to CA, another bottom-up approach used for multidimensional biofilm modelling of which several examples may be found in the literature (Wimpenny and Colasanti, 1997; Picioreanu *et al*., 1998; Noguera *et al*., 1999; Chang *et al*., 2003; Hunt *et al*., 2003; Laspidou and Rittmann, 2004). The fundamental difference between the IbM used in the framework and CA lays in the biomass representation. In CA methods the biomass is represented on a grid (usually rectangular), as opposed to the agent-based representation of the IbM that uses particles located anywhere in space. As a consequence of the distinct methods of describing the biomass and in particular in the biomass spreading rules used, there are differences in the results of simulations of equivalent systems carried out with the two approaches (Kreft *et al*., 2001). Such differences are also in the root of a number of drawbacks of numerical nature that are characteristic to the CA approach (Eberl *et al*., 2001). Most importantly, it was reported previously that IbM is more suitable to the modelling of multispecies biofilms than CA (Picioreanu *et al*., 2004) and that IbM has greater potential to address questions about the relationship of microscopic and macroscopic properties in mixed-population systems (Kreft *et al*., 2001; Van Loosdrecht *et al*., 2002).

Continuum approaches for multidimensional modelling of biofilms may also be found in the literature (Dockery

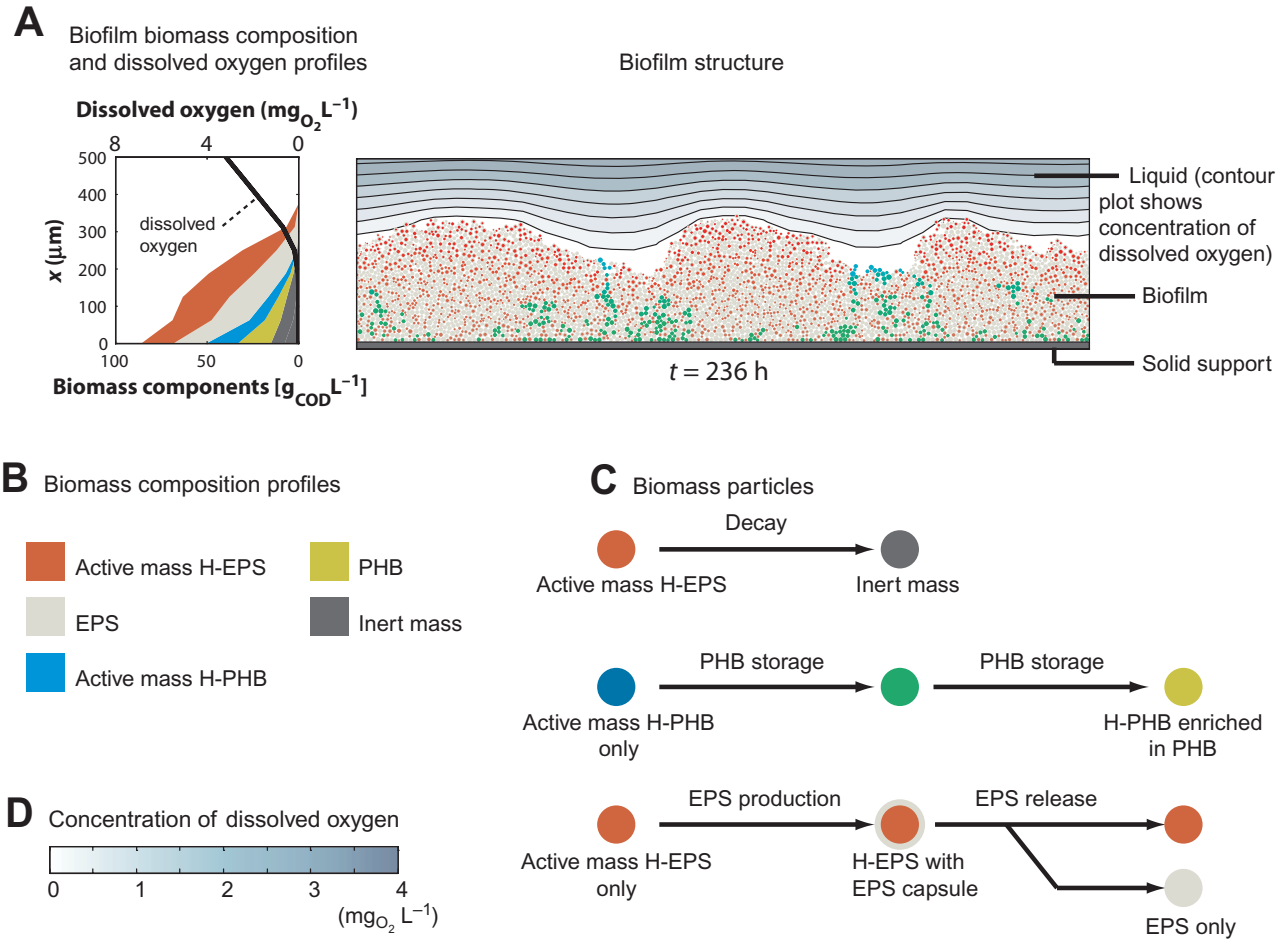

Fig. 5. Key for Figs 6 and 7, which show biofilm structure results from 2D simulations of the case study.
A. Left panel shows the profiles of the average dissolved oxygen concentration (black line) and the average biomass composition (area plots) along the depth of the biofilm. The distance to the solid substratum (in µm) is *x*. The right panel shows the circular-shaped agents at a given time in the simulation and the spatial fields of the concentration of dissolved oxygen.
B. The colour code used in the profiles of biomass composition.
C. The colour code used for agents shown in the biofilm structure representations.
D. The colour code used for the 2D field of concentration of dissolved oxygen shown together with the biofilm structure representation.

and Klapper, 2001; Eberl *et al.*, 2001; Alpkvist *et al.*, 2004). These approaches are distinct from bottom-up approaches by using a homogeneous representation of the biomass and by having the dynamics of biomass spreading modelled by differential equations widely used in physics. Therefore, continuum approaches have the advantage that the method for biomass spreading used is fully deterministic, therefore it can be analysed numericaly. This is in contrast to bottom-up approaches, such as the IbM, where biomass spreading is stochastic. Furthermore, the biofilm description as a viscous, incompressible fluid (Dockery and Klapper, 2001) is intuitively more suitable to model the gel-like EPS matrix than the approach adopted here, where EPS is incorporated in the IbM. However, in spite of its conceptual attractiveness, to the best of our knowledge, no example of multidimensional continuum model of a multispecies biofilm exists presently. All applications of this approach are presently limited to homogeneous representations of biomass.

The fact that several approaches for multidimensional modelling of biofilms can be found in the literature is indicative of the booming interest in the field. This interest is both inspired by the stimulating results achieved by pioneer work and facilitated by the increasing availability of affordable computational power. Simulations that previously required high-end mainframe computers run nowadays in ordinary desktop PCs. However, the increasing number of different modelling implementations, at the same time, reflects the immaturity of this relatively recent research field. A standardization of methods used for multidimensional modelling is highly desirable for the near future. The adoption of a common modelling framework

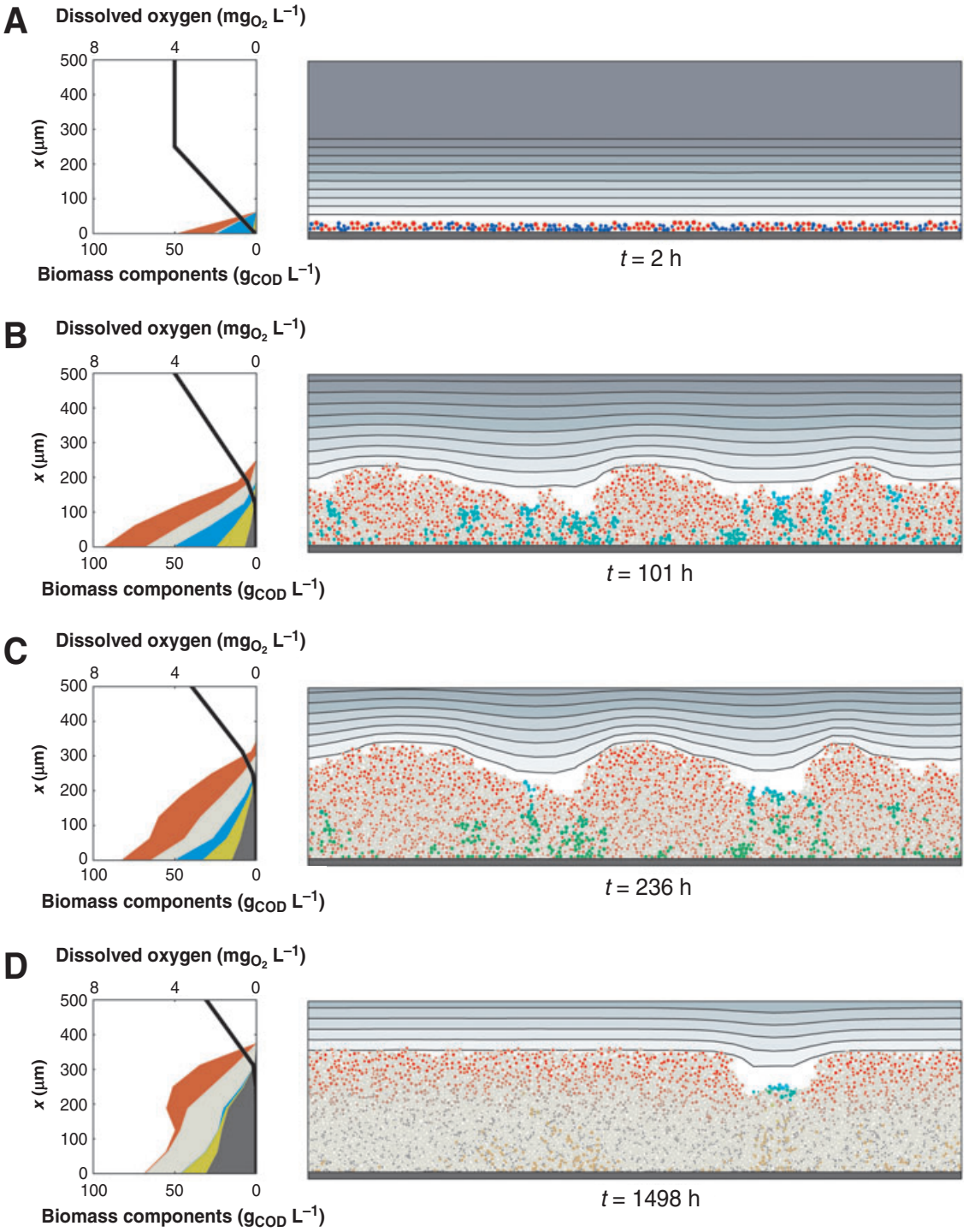

Fig. 6. Continuous feeding case: Vertical distribution of biomass composition (left hand side) and biofilm structure (right hand side) from 2D simulations at times 1 h (A), 103 h (B), 238 h (C) and 1500 h (D). See legend in Fig. 5. In the continuous feeding case shown here EPS producer (H-EPS) has a competitive advantage over PHB producer (H-PHB). This advantage is a consequence of the faster spreading of H-EPS organisms that, by producing EPS (a low density polymer), creates a larger volume when compared with PHB (intracellular storage polymer of higher density than EPS) for the same biomass of polymer produced. By spreading faster, EPS producers occupy a superior position in the biofilm structure, taking advantage of the higher oxygen concentrations at the top. In the simulations, the concentration boundary layer follows in time the biofilm growth, being always located at a distance $L_c = 100$ μm of the highest biofilm feature. The smooth surface developed by the biofilm at the end of the simulation is not imposed by cutting the biofilm, but it is results from the balance between biofilm growth and the detachment implemented using F_{det} proportional to the square of the distance to the surface and decreasing with the local biofilm density. 2D simulations were started with 30 particles of each species (H-EPS and H-PHB) in the system.

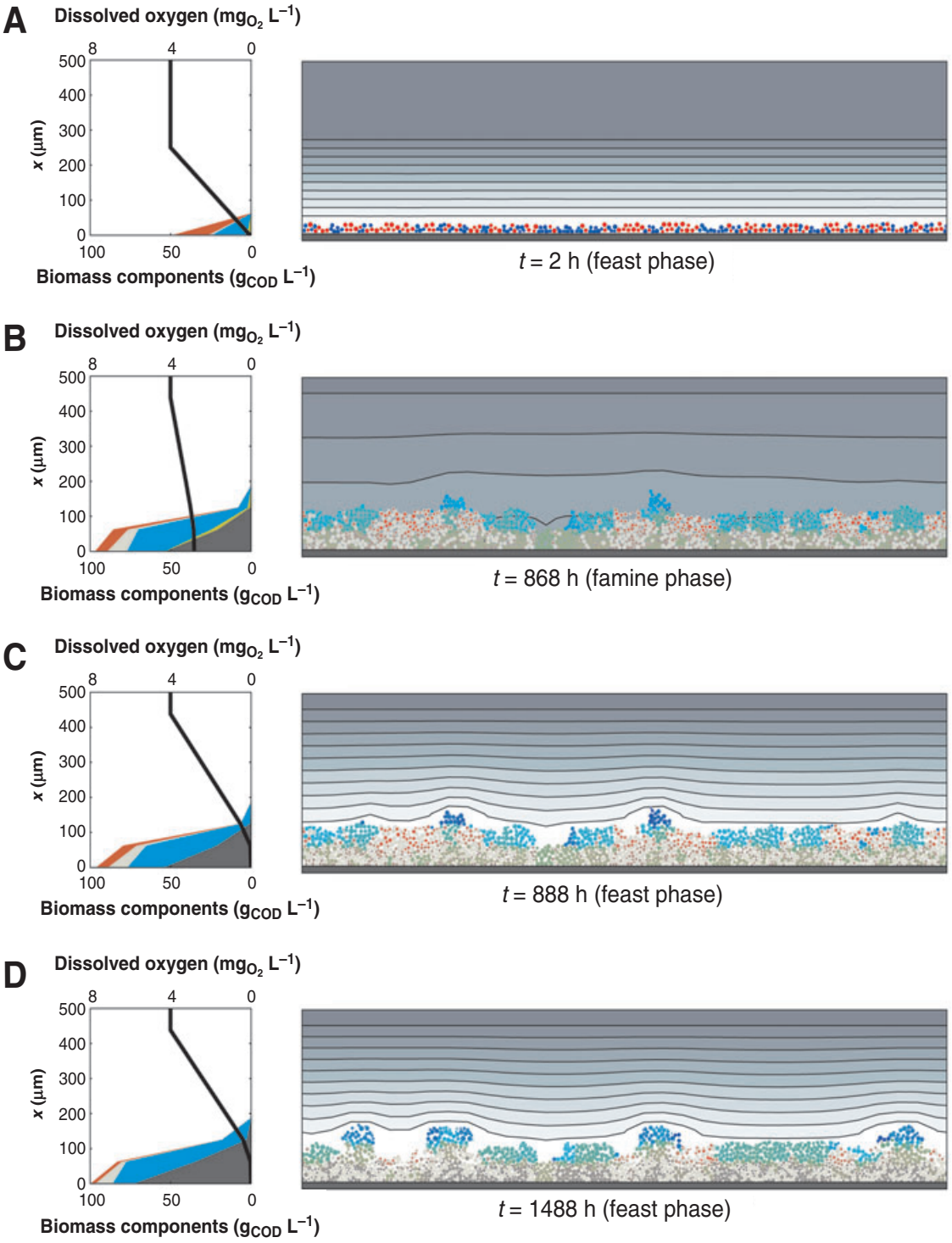

Fig. 7. Feast/famine cycles case: Results from 2D simulations at times 1 h (A), 868 h (B), 888 h (C) and 1488 h (D). See legend in Fig. 5. Results show that selection for PHB producers may be achieved by a feast/famine regime. H-PHB organisms accumulate PHB internal storage during the feast phase, when $C_S = 0.5$ g_{COD} l^{-1}, which is consumed during the famine phase, when $C_S = 0$. At the beginning of each famine phase (as seen in the biomass composition profile in B) the biofilm shows high quantities of PHB and oxygen profiles demonstrate that growth is not oxygen-limited, because of the low (0) bulk concentration of substrate. At the beginning of a feast phase (as seen in the biomass composition profile in (C), however, all PHB was consumed and growth is once again oxygen-limited. In this phase, organisms take advantage of the high concentration of substrate to grow and produce polymers. At the end of the simulation (Fig. 7D), the biofilm is enriched in PHB accumulating organisms when compared with the continuous-feeding case at the same time (Fig. 6D). Animations of the simulations shown here are available at our website (Xavier *et al.*, 2004a).

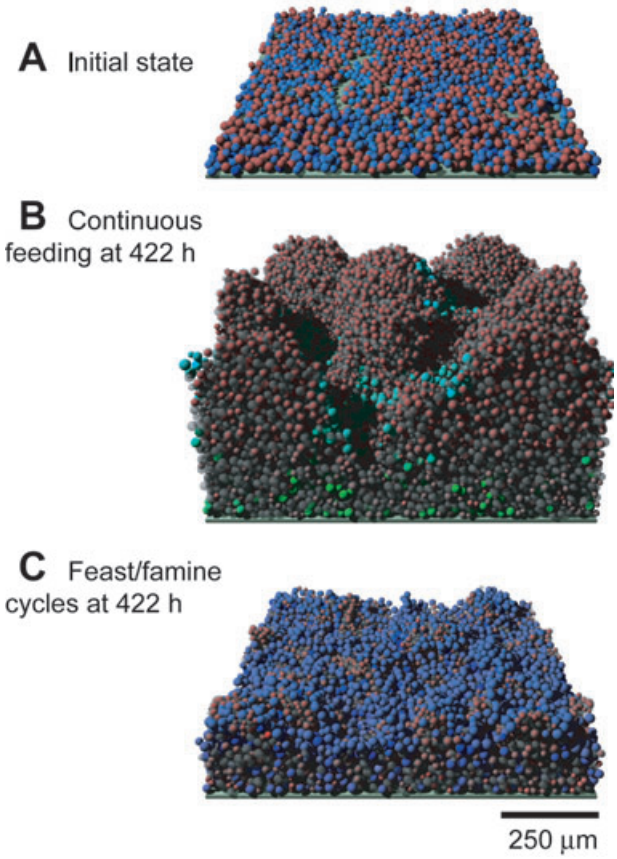

Fig. 8. Biofilm structures from 3D simulations of the case study presented. Colour coding of biomass agents (spherical particles) is the same as used in the 2D representations (explained in Fig. 5C).
A. Initial state used for simulations of both the continuous feeding and the feast/famine cases, showing the inoculated plate representing an area of $1000 \times 1000\ \mu m^2$.
B. Biofilm structure after 422 h for the continuous feeding case, showing predominance of H-EPS over H-PHB.
C. Biofilm structure for the feast/famine case after 422 h of growth, showing predominance of H-PHB over H-EPS.

such as the one proposed here would certainly assist in such standardization. By combining many of the most advanced features of bottom-up multidimensional modelling approaches into a software library that is readily available, we hope that the present work will stimulate the creation of new biofilm models.

In spite of the fact that many challenges of computational or numerical nature have been overcome in recent advances, including this contribution, there is a lack of experimental data to allow the unbiased description of important properties of the system, e.g. EPS physical properties. This lack of parameters for realistic modelling of biofilm systems probably constitutes the most important factor presently limiting the creation of new reliable biofilm models. Confocal laser scanning microscopy (CLSM) of biofilms (Lawrence *et al.*, 1991) may be the most indicated tool to overcome this obstacle by providing necessary information for biofilm models. A comparative study of biofilm structure obtained from IbM simulations and structure observed using CLSM imaging of biofilms grown in laboratory flowcells has demonstrated that this technique provides an ideal source of data to be used for biofilm models (Xavier *et al.*, 2004b), thanks to its dynamic but non-destructive characteristics. An important result from that comparative study was to show that, in spite of biases introduced by IbM such as representing biomass as being composed by spherically shaped particles, simulations were still able to reproduce biofilm structure observed experimentally, as quantified by a set of morphological parameters. Further potential of CLSM to provide data for modelling lies in multichannel image acquisition, which provides 3D information concerning multiple components of the biofilm such as EPS and bacteria of different species or in different development stages (Lawrence and Neu, 1999).

Notation

Symbol	Definition [Dimension]
γ_{in}	Sign factor of reaction i relative to species n (solute or particulate). Has a value +1 if the n is produced in the reaction and −1 if it is consumed [dimensionless]
Δt	Time step for one iteration of biomass dynamics [T]
Δt_1	Time step constraint set on the individual scale [T]
Δt_2	Time step constraint set on the biofilm scale [T]
Δt_3	Time step constraint set on the global system scale [T]
μ^{max}	Maximum specific growth rate of biomass [$M_p\ M_p^{-1} T^{-1}$]
ρ_m	Specific mass of particulate species m (solute or particulate) [M_m (L^3 of particle)$^{-1}$]
ϕ_j	Factor for dependency of specific rate of a reaction on component j [dimensionless]
$\phi_{I,m}$	Rate inhibition factor of species m [dimensionless]
$\phi_{M,m}$	Rate saturation factor of species m [dimensionless]
$A_{carrier}$	Total carrier area (biofilm support) in the system [L^2]
C_i	Concentration of species i (solute or particulate) [$M_i\ L^{-3}$]
C_S^{in}	Input concentration of solute species s in the system [$M_S\ L^{-3}$]
C_S^{bulk}	Bulk concentration of solute species s [$M_S\ L^{-3}$]
C_S^{fam}	Bulk concentration of solute s in famine period [$M_S\ L^{-3}$]
C_S^{feast}	Bulk concentration of solute s in feast period [$M_S\ L^{-3}$]

D_S	Diffusivity of solute species s [$L^2\ T^{-1}$]
F_{det}	Detachment speed function [$L\ T^{-1}$]
$f_{EPS,excretion}$	Critical volume fraction of EPS, for EPS excretion [dimensionless]
f_V	Fraction of volume defined for iteration time step constraint Δt_2 [dimensionless]
K_j	Monod saturation constant in $\phi_{M,j}$ or inhibition constant in $\phi_{I,j}$ [$M_j\ L^{-3}$]
L_c	Thickness of concentration boundary layer [L]
L_x	Depth of computational domain (vertical dimension) [L]
L_y, L_z	Horizontal dimensions of computational domain [L, L]
M_p	Mass of particulate species p in a biomass particle [M_p particle^{-1}]
$\boldsymbol{n}(\boldsymbol{x})$	Vector normal to the biofilm surface at location $\boldsymbol{x}$ [dimensionless]
Q	Volumetric flow rate [$L^3\ T^{-1}$]
q_i	Specific rate for reaction i, defined in reference to species m (solute or particulate) and mediated by particulate species p [$M_m\ M_p^{-1}\ T^{-1}$]
q_i^{max}	Maximum specific rate for reaction i, defined in reference to species m (solute or particulate) and mediated by particulate species p [$Mm\ M_p^{-1}\ T^{-1}$]
$R(C_S^{bulk})$	Global conversion rate of solute species s in the system [$M_S\ L^{-3}\ T^{-1}$]
$R_{division}$	Critical radius for biomass particle division [L]
r_i	Rate for reaction i defined in reference to species m (solute or particulate) [$M_m\ L^{-3}\ T^{-1}$]
R_n	Net rate for species n (solute or particulate) [$M_n\ L^{-3}\ T^{-1}$]
$R_{particle}$	Radius of biomass particle (agent) [L]
V_{comp}	Volume of the computational volume [L^3]
$V_{particle}$	Volume of a biomass particle (agent) [L^3]
V_{sys}	Total volume of the full-scale system [L^3]
$\boldsymbol{x}$	Location of a point (defined in 2D or 3D) located on the biofilm interface [L]
Y_{nm}^i	Yield coefficient of species n (solute or particulate) on species m (solute or particulate) in reference to reaction i [$M_n\ M_m^{-1}$]

Acknowledgements

J. B. Xavier thankfully acknowledges financial support by the FCT/MCTES, Portugal, through the Grant SFRH/BPD/11485/2002.

References

Alpkvist, E., Overgaard, N.C., Gustafsson, S., and Heyden, A. (2004) A new mathematical model for chemotactic bacterial colony growth. *Water Sci Technol* **49:** 187–192.

Anderson, A.J., and Wynn, J.P. (2001) Microbial polyhydroxyalkanoates polysaccharides and lipids. In *Basic Biotechnology*. Ratledge, C., and Kristiansen, B. (eds). Cambridge, UK: Cambridge University Press, pp. 325–348.

Beuling, E.E., van Dusschoten, D., Lens, P., van den Heuvel, J.C., Van As, H., and Ottengraf, S.P.P. (1998) Characterization of the diffusive properties of biofilms using pulsed field gradient-nuclear magnetic resonance. *Biotechnol Bioeng* **60:** 283–291.

Beuling, E.E., van den Heuvel, J.C., and Ottengraf, S.P.P. (2000) Diffusion coefficients of metabolites in active biofilms. *Biotechnol Bioeng* **67:** 53–60.

Beun, J.J. (2001) PHB metabolism and N-removal in sequencing batch granular sludge reactors. PhD Thesis. Delft, the Netherlands: Delft University of Technology, Department of Biotechnology. 156 pages.

Beun, J.J., Dircks, K., Van Loosdrecht, M.C.M., and Heijnen, J.J. (2002) Poly-beta-hydroxybutyrate metabolism in dynamically fed mixed microbial cultures. *Water Res* **36:** 1167–1180.

Chang, I., Gilbert, E.S., Eliashberg, N., and Keasling, J.D. (2003) A three-dimensional, stochastic simulation of biofilm growth and transport-related factors that affect structure. *Microbiol-SGM* **149:** 2859–2871.

Characklis, W.G. (ed.) (1990) *Biofilm Processes*. New York, USA: Wiley Interscience.

Characklis, W.G., and Marshall, K.C. (eds) (1990) *Biofilms: A Basis for an Interdisciplinary Approach*. New York, USA: Wiley Interscience.

Dockery, J., and Klapper, I. (2001) Finger formation in biofilm layers. *SIAM J Appl Math* **62:** 853–869.

Eberl, H.J., Picioreanu, C., Heijnen, J.J., and Van Loosdrecht, M.C.M. (2000) A three-dimensional numerical study on the correlation of spatial structure, hydrodynamic conditions, and mass transfer and conversion in biofilms. *Chem Eng Sci* **55:** 6209–6222.

Eberl, H.J., Parker, D.F., and Van Loosdrecht, M.C.M. (2001) A new deterministic spatio-temporal continuum model for biofilm development. *J Theor Med* **3:** 161–175.

Gujer, W., and Larsen, T.A. (1995) The implementation of biokinetics and conservation principles in ASIM. *Water Sci Technol* **31:** 257–266.

Horn, H., Neu, T.R., and Wulkow, M. (2001) Modelling the structure and function of extracellular polymeric substances in biofilms with new numerical techniques. *Water Sci Technol* **43:** 121–127.

Hunt, S.M., Hamilton, M.A., Sears, J.T., Harkin, G., and Reno, J. (2003) A computer investigation of chemically mediated detachment in bacterial biofilms. *Microbiol-SGM* **149:** 1155–1163.

Klapper, I. (2004) Effect of heterogeneous structure in mechanically unstressed biofilms on overall growth. *Bull Math Biol* **66:** 809–824.

Kreft, J.U. (2004) Biofilms promote altruism. *Microbiol-SGM* **150:** 2751–2760.

Kreft, J.U., and Wimpenny, J.W.T. (2001) Effect of EPS on biofilm structure and function as revealed by an individual-based model of biofilm growth. *Water Sci Technol* **43:** 135–141.

Kreft, J.U., Booth, G., and Wimpenny, J.W.T. (1998) BacSim, a simulator for individual-based modelling of bacterial colony growth. *Microbiology* **144:** 3275–3287.

Kreft, J.U., Picioreanu, C., Wimpenny, J.W.T., and Van Loosdrecht, M.C.M. (2001) Individual-based modelling of biofilms. *Microbiol-SGM* **147:** 2897–2912.

Kuenen, J.G., Jorgensen, B.B., and Revsbech, N.P. (1986) Oxygen microprofiles of trickling filter biofilms. *Water Res* **20:** 1589–1598.

Kwok, W.K., Picioreanu, C., Ong, S.L., Van Loosdrecht, M.C.M., Ng, W.J., and Heijnen, J.J. (1998) Influence of biomass production and detachment forces on biofilm structures in a biofilm airlift suspension reactor. *Biotechnol Bioeng* **58:** 400–407.

Laspidou, C.S., and Rittmann, B.E. (2004) Modeling the development of biofilm density including active bacteria, inert biomass, and extracellular polymeric substances. *Water Res* **38:** 3349–3361.

Lawrence, J.R., and Neu, T.R. (1999) Confocal laser scanning microscopy for analysis of microbial biofilms. *Methods Enzymol* **310:** 131–144.

Lawrence, J.R., Korber, D.R., Hoyle, B.D., Costerton, J.W., and Caldwell, D.E. (1991) Optical sectioning of microbial biofilms. *J Bacteriol* **173:** 6558–6567.

Morgenroth, E., and Wilderer, P.A. (1999) Controlled biomass removal – the key parameter to achieve enhanced biological phosphorus removal in biofilm systems. *Water Sci Technol* **39:** 33–40.

Morgenroth, E., and Wilderer, P.A. (2000) Influence of detachment mechanisms on competition in biofilms. *Water Res* **34:** 417–426.

Noguera, D.R., and Picioreanu, C. (2004) Results from the multi-species Benchmark Problem 3 (BM3) using two-dimensional models. *Water Sci Technol* **49:** 169–176.

Noguera, D.R., Pizarro, G., Stahl, D.A., and Rittmann, B.E. (1999) Simulation of multispecies biofilm development in three dimensions. *Water Sci Technol* **39:** 503–510.

Noguera, D.R., Pizarro, G., and Clapp, L.W. (2000) Mathematical modeling of trichloroethylene (TCE) degradation in membrane-attached biofilms. *Water Sci Technol* **41:** 239–244.

Picioreanu, C., and Van Loosdrecht, M.C.M. (2003) Use of mathematical modelling to study biofilm development and morphology. In *Biofilms in Medicine, Industry and Environmental Biotechnology – Characteristics, Analysis and Control.* Lens, P., O'Flaherty, V., Moran, A.P., Stoodley, P., and Mahony, T. (eds). London: IWA Publishing, pp. 413–437.

Picioreanu, C., Van Loosdrecht, M.C.M., and Heijnen, J. (1998) Mathematical modelling of biofilm structure with a hybrid differential-discrete cellular automaton approach. *Biotech Bioeng* **58:** 101–116.

Picioreanu, C., Van Loosdrecht, M.C.M., and Heijnen, J.J. (1999) Discrete-differential modelling of biofilm structure. *Water Sci Technol* **39:** 115–122.

Picioreanu, C., Van Loosdrecht, M.C.M., and Heijnen, J.J. (2000a) A theoretical study on the effect of surface roughness on mass transport and transformation in biofilms. *Biotechnol Bioeng* **68:** 355–369.

Picioreanu, C., Van Loosdrecht, M.C.M., and Heijnen, J.J. (2000b) Effect of diffusive and convective substrate transport on biofilm structure formation: a two-dimensional modeling study. *Biotechnol Bioeng* **69:** 504–515.

Picioreanu, C., Van Loosdrecht, M.C.M., and Heijnen, J.J. (2001) Two-dimensional model of biofilm detachment caused by internal stress from liquid flow. *Biotechnol Bioeng* **72:** 205–218.

Picioreanu, C., Kreft, J.U., and Van Loosdrecht, M.C.M. (2004) Particle-based multidimensional multispecies model. *Appl Environ Microbiol* **70:** 3024–3040.

Press, W.H., Flannery, B.P., Teukolsky, S.A., and Vetterling, W.T. (1997) *Numerical Recipes in C: The Art of Scientific Computing*. Cambridge, UK: Cambridge University Press.

Reichert, P. (1994) Aquasim – a tool for simulation and data-analysis of aquatic systems. *Water Sci Technol* **30:** 21–30.

Reis, M.A.M., Serafim, L.S., Lemos, P.C., Ramos, A.M., Aguiar, F.R., and Van Loosdrecht, M.C.M. (2003) Production of polyhydroxyalkanoates by mixed microbial cultures. *Bioprocess Biosyst Eng* **25:** 377–385.

Rittmann, B.E., Pettis, M., Reeves, H.W., and Stahl, D.A. (1999) How biofilm clusters affect substrate flux and ecological selection. *Water Sci Technol* **39:** 99–105.

Rittmann, B.E., Schwarz, A.O., Eberl, H.J., Morgenroth, E., Perez, J., van Loosdrecht, M., and Wanner, O. (2004) Results from the multi-species Benchmark Problem (BM3) using one-dimensional models. *Water Sci Technol* **49:** 163–168.

Stewart, P.S. (1993) A model of biofilm detachment. *Biotechnol Bioeng* **41:** 111–117.

Stoodley, P., Boyle, J.D., De Beer, D., and Lappin-Scott, H.M. (1999) Evolving perspectives of biofilm structure. *Biofouling* **14:** 75–90.

Van Loosdrecht, M.C.M., and Heijnen, J.J. (2002) Modelling of activated sludge processes with structured biomass. *Water Sci Technol* **45:** 13–23.

Van Loosdrecht, M.C.M., Eikelboom, D., Gjaltema, A., Mulder, A., Tijhuis, L., and Heijnen, J.J. (1995) Biofilm structures. *Water Sci Technol* **32:** 35–43.

Van Loosdrecht, M.C.M., Pot, M.A., and Heijnen, J.J. (1997) Importance of bacterial storage polymers in bioprocesses. *Water Sci Technol* **35:** 41–47.

Van Loosdrecht, M.C.M., Heijnen, J.J., Eberl, H.J., Kreft, J.U., and Picioreanu, C. (2002) Mathematical modelling of biofilm structures. *Antonie Van Leeuwenhoek* **81:** 245–256.

Wanner, O., and Gujer, W. (1986) A multispecies biofilm model. *Biotech Bioeng* **28:** 314–328.

Wanner, O., and Reichert, P. (1996) Mathematical modeling of mixed-culture biofilms. *Biotechnol Bioeng* **49:** 172–184.

Wasche, S., Horn, H., and Hempel, D.C. (2002) Influence of growth conditions on biofilm development and mass transfer at the bulk/biofilm interface. *Water Res* **36:** 4775–4784.

Wimpenny, J.W.T., and Colasanti, R. (1997) A unifying hypothesis for the structure of microbial biofilms based on cellular automaton models. *FEMS Microbiol Ecol* **22:** 1–16.

Xavier, J.B., Picioreanu, C., and Van Loosdrecht, M.C.M. (2004a) *Support material for 'A Framework for Multidimensional Modelling of Activity and Structure of Multispecies Biofilms'* [WWW document]. URL http://www.biofilms.bt.tudelft.nl/frameworkMaterial/ [accessed on 5 March 2005].

Xavier, J.B., Picioreanu, C., and Van Loosdrecht, M.C.M.

(2004b) Assessment of three-dimensional biofilm models through direct comparison with confocal microscopy imaging. *Water Sci Technol* **49:** 177–185.

Zhang, X.Q., and Bishop, P.L. (2001) Spatial distribution of extracellular polymeric substances in biofilms. *J Environ Eng-ASCE* **127:** 850–856.

Zhang, T.C., Bishop, P.L., and Gibbs, J.T. (1994) Effect of roughness and thickness of biofilms on external mass transfer resistance. In *Critical Issues in Water and Wastewater Treatment National Conference in Environmental Engineering.* Ryan, J.N. and Edwards, M. (eds). New York, USA: ASCE, pp. 593–600.